PERGAMON

International Journal of Solids and Structures 39 (2002) 5345–5369

INTERNATIONAL JOURNAL OF SOLIDS and STRUCTURES

www.elsevier.com/locate/ijsolstr

A study of transient elastic wave propagation in a bimaterial modeling the thorax

Quentin Grimal, Salah Naili *, Alexandre Watzky

Faculté des Sciences et Technologie, Laboratoire de Mécanique Physique, CNRS UMR 7052 B2OA, Université Paris XII-Val de Marne 61, Avenue du Général de Gaulle, 94010 Créteil Cédex, France

Received 11 June 2001

Abstract

The transient response of an elastic bimaterial, made out of a "hard" medium and a "soft" medium, welded at a plane interface, have been investigated by using an integral transform technique that permits isolation of the pressure and shear waves contributions to the wave-field. The method, often referred to as the generalized ray/Cagniard-de Hoop method (GR/CdH), is briefly presented. The wave motion is generated alternatively by a buried point source of strain rate and by a point force perpendicular to the free surface of the bimaterial. New simplified solutions are derived for points located on the axis perpendicular to the interfaces and passing through the source. Owing to the formalism, an approximation to the strain energy is shown to be readily obtained. The numerical schemes for the implementation of the exact three-dimensional GR/CdH are presented. Numerical examples are concerned with the propagation of an impact wave in the thorax modeled as a bimaterial (thoracic wall–lung). The effects of the weak coupling between the thoracic wall and the lung are investigated. The distributions of transient strain energies, respectively carried by the pressure and the shear waves in the media representing the lung, are plotted.

Keywords: Transient; Wave; Layered media; Cagniard-de Hoop; Impact; Thorax; Generalized rays

1. Introduction

The study of transient elastic waves in layered media is of interest for many applications. In the past 10 decades, geophysicians have developed powerful analytical and numerical methods to solve problems derived from seismology; these methods have then been used in other fields of mechanical engineering such as non-destructive evaluation of composites and ocean acoustics.

Exact solutions—including far field and near field terms—in the time domain for two and three-dimensional elastodynamics problems in stratified media can be derived with the help of the generalized ray/Cagniard-de Hoop (GR/CdH) method (some relevant references for these techniques are Kennett (1983) and Pao and Gajewski (1977)). The GR theory splits the solution for the wave motion at some point

* Corresponding author. Tel.: +33-1-45-17-14-45; fax: +33-1-45-17-14-33.
E-mail addresses: grimal@univ-paris12.fr (Q. Grimal), naili@univ-paris12.fr (S. Naili), watzky@univ-paris12.fr (A. Watzky).

0020-7683/02/$ - see front matter
PII: S0020-7683(02)00400-6

Nomenclature

$\mathbf{b} = (v_1, v_2, v_2, -\sigma_{13}, -\sigma_{23}, -\sigma_{33})^{\mathrm{T}}$	motion stress vector (unknown vector)
c_{P}	pressure wave speed ($\mathrm{m\,s^{-1}}$)
c_{S}	shear wave speed ($\mathrm{m\,s^{-1}}$)
E_d	strain energy per unit volume ($\mathrm{kg\,m^{-1}\,s^{-2}}$)
h_1	distance from the source to the interface (m)
h_2	distance from the interface to the receiver (m)
h_{ij}	component of the source of strain rate tensor ($\mathrm{s^{-1}}$)
pk_i	spatial horizontal Fourier transformation parameter (horizontal wave numbers) ($\mathrm{m^{-1}}$)
p	time Laplace transformation parameter ($\mathrm{s^{-1}}$)
$\mathbf{P}$	energy flux vector (Poynting vector) ($\mathrm{kg\,s^{-3}}$)
s_{P}	pressure wave slowness ($\mathrm{s\,m^{-1}}$)
s_{S}	shear wave slowness ($\mathrm{s\,m^{-1}}$)
$T_{\alpha\to\beta}$	transmission coefficient [1]
v_i	component of the particle velocity ($\mathrm{ms^{-1}}$)
x_i	spatial coordinates (m)
σ_{ij}	component of the Cauchy stress tensor (Pa)
λ, μ	Lamé coefficients (Pa)
ρ	density of mass ($\mathrm{kg\,m^{-3}}$)
$\phi(t)$	source pulse shape [1]
∂_i	partial differentiation with respect to the spatial coordinate x_i ($\mathrm{m^{-1}}$)
∂_t	partial differentiation with respect to time ($\mathrm{s^{-1}}$)
$\tilde{}$	denotes Fourier–Laplace transform domain quantities
$\hat{}$	denotes Laplace transform domain quantities
$\mathfrak{I}$	imaginary part of a quantity
$\mathfrak{R}e$	real part of a quantity

of the medium (called the receiver) in a sum of contributions; each contribution is associated with a "GR path", i.e., with a succession of transmissions and reflections at interfaces between the source and the receiver and at each interface, a wave is reflected or transmitted with or without mode conversion. Finally, a GR is defined both by a path and by a sequence of modes of propagation (longitudinal or transverse polarization), i.e., one mode per layer crossed. The decomposition in GR is performed in a tranformed domain involving Fourier and/or Laplace variables, dual of the space and time variables. The CdH method applies to each integral transform representation of contributions to the solution—that is, to each GR. In essence, it is a mathematical trick to avoid integration over the frequency (or over the wave number) required to transform the solutions back to the space–time domain.

Although the *exact* three-dimensional GR/CdH method for layered media and associated formalisms are extensively described in the literature devoted to seismology (see Van Der Hijden, 1987; Kennett, 1983; Aki and Richard, 1980; Pao and Gajewski, 1977), they seem to be rarely used for other engineering applications; as a matter of consequence, little information could be found on the numerical implementation of the method. For instance, some computer codes designed to generate synthetic seismograms only use an asymptotic approximation (Herrmann, 2001) valid far from the source. The numerical implementation of asymptotic solutions—far field or high frequency (see Kennett, 1983; Van Der Hijden, 1987)—is simplified in comparison with the implementation of exact solutions. However, many closed form analytical solutions

can be derived, for some specific sources and simple configurations, with the CdH method; for arbitrary layered media, the GR/CdH method can be used to compute fast and accurate seismograms (however, the method is not recommended if the number of layers is important).

Other methods to transform the solutions back to the space–time domain are sometimes used but they involve a numerical integration over the frequency (see Aki and Richard, 1980; Cetinkaya and Vakaris, 1996); this requires extensive computations and often leads only to approximate solutions (Kennett, 1983).

In what follows, we will use the term "bimaterial" to designate the simplest "stratified" medium: two media separated by a plane interface. In this paper, theory and numerical results are concerned with a bimaterial; however, the formalism and the numerical implementation proposed are suited to arbitrary plane layered media. We will consider two bimaterials associated with given loadings: Case I (Fig. 1a) consists of two homogeneous semi-infinite media, media 1 and 2, a buried explosion source (source of strain rate) placed in medium 1 generates the wave motion; in Case II (Fig. 1b), medium 1 is limited by a free surface where a point force, normal to the surface, generates the wave motion. One medium is semi-infinite and the other, in which the source is introduced, is whether semi-infinite (Case I) or limited by a free surface (Case II). At the interface, the media are welded. Ma and Huang (1996) obtained exact transient two-dimensional closed form solutions for a point force acting at a depth in a bimaterial (two semi-infinite media) but we do not know of any closed form analytical solutions for the equivalent three-dimensional problem.

The aim of this paper is to present new developments associated with the GR/CdH method and to introduce an original field for its application (the paper is an extension of a note (Grimal et al., 2001) in which preliminary results were presented). For an arbitrary layered medium, we derive a simplified three-dimensional solution for points located on the $\mathbf{x}_3$-axis of Fig. 1; for a bimaterial, we give the closed form analytical solution in this case. This solution may be used to get an insight into the physical response of a bimaterial but for the present study, it has been useful to validate the computer code. Since references concerning the numerical implementation of the *exact* three-dimensional GR/CdH method are rare (Pao and Gajewski, 1977) and since we could not find any using Van Der Hijden's (1987) formalism—using a Cartesian reference frame—, we briefly present the numerical schemes used in our computer code. We point out that, owing to the formalism, an approximation of the strain energy carried by the waves can be readily

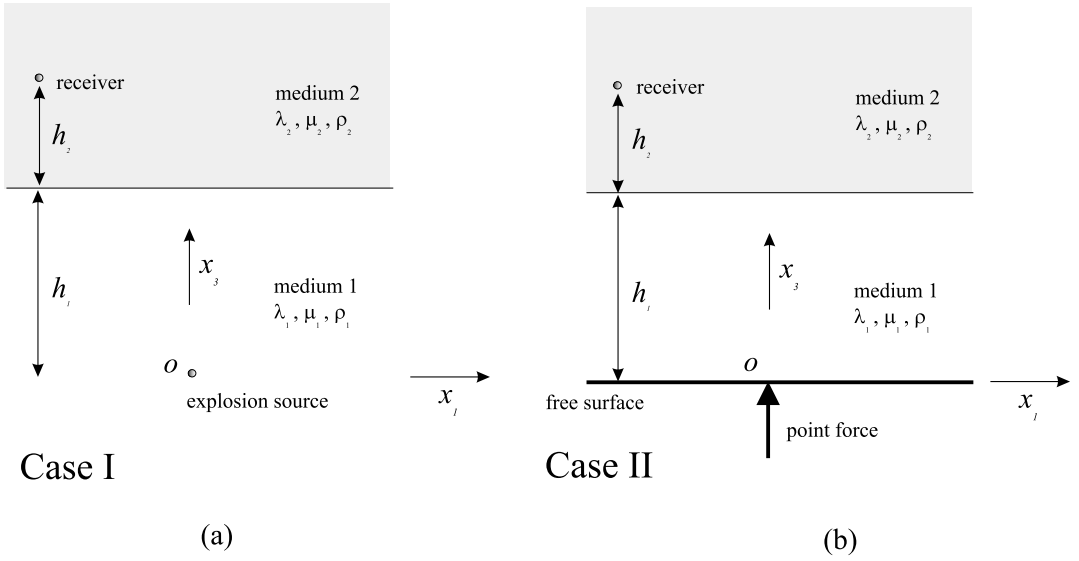

Fig. 1. Configuration and coordinate system: (a) explosion source (Case I); (b) point force at the free surface (Case II).

obtained from the energy flux vector. Indeed, formalisms used to solve three-dimensional wave propagation problems in layered media—propagation or scattering matrix methods—make use of six unknown variables for which the problem is solved; they can be chosen to be the three components of the particle velocity, together with the three components of the stress tensor which are continuous across the interfaces (the motion-stress vector), so that an inner product yields the energy flux vector (Poynting vector) in the direction normal to the interface.

In the present work, we have been interested in a biomechanical application: the propagation of waves in the thorax following a non-penetrating impact. This is of interest to the defense industry concerned with high velocity impacts (design of bulletproof jackets), and to the automotive industry concerned with lower velocity impacts (crash safety systems). The necessity for investigations on the interaction of stress waves with thoracic tissues has been underlined by Fung et al. (1988), Yen et al. (1988) and Fung (1990): the impact wave is supposed to play an important role in the occurrence of injuries, i.e., in the injury mechanisms. Pressure and shear waves are thought to play different roles in the injury mechanisms; the GR theory is thus relevant for the study of the wave propagation since it makes it possible to differentiate the modes of propagation of energy. Regarding the biomechanical application, the strain energy is a most useful quantity for characterizing the wave propagation because it is a scalar that globally represents the state of stress of the medium (no specific component of stress or strain is associated with a risk of injury). Numerical examples are concerned with a bimaterial media modeling the thorax: medium 1 stands for the thoracic wall and medium 2 represents the lung. Computations for Cases I and II have allowed us to localize the energy carried by the shear and pressure waves in the medium representing the lung.

With this brief review as background, we present in Section 2 a description of the method of solution and we show how an approximation to the strain energy can be obtained from the components of the Poynting vector. In Section 3, we derive an analytical solution valid at some points of a bimaterial and we show how it extends to a layered medium. Section 4 is devoted to the computational schemes. Numerical examples for the biomechanical application are presented in Section 5.

2. General formulation

In this section, we present, for the sake of completeness, the exact three-dimensional GR/CdH method. We essentially follow Van Der Hijden (1987) for the presentation of the formalism. Some details and discussions of the procedures have been omitted here and will be found in the aforementioned reference.

2.1. The elastodynamics problem

2.1.1. Configuration and definitions

The model configuration (Fig. 1) consists of two media, media 1 and 2, separated by a plane interface. Each layer is homogeneous, isotropic and obeys Hooke's law; for the characterization of the elastic properties, the Lamé constants λ and μ are used, the volume density of mass is denoted by ρ. The position is specified through the coordinates (x_1, x_2, x_3) with respect to a Cartesian reference frame $R(O, \mathbf{x}_1, \mathbf{x}_2, \mathbf{x}_3)$ where O is the origin and $(\mathbf{x}_1, \mathbf{x}_2, \mathbf{x}_3)$ is an orthonormal basis for the space; the $\mathbf{x}_3$-axis is taken to be ascending vertical and perpendicular to the interface. The elastic wave motion will be characterized in R by the components σ_{ij} of the Cauchy stress tensor and by the components v_i of the particle velocity. The media are unbounded in the x_1 and x_2 directions. Medium 2 is semi-infinite; for medium 1, we will consider two cases: (i) semi-infinite medium (Case I) and (ii) free surface condition at $x_3 = 0$: $\sigma_{13}(x_1, x_2, 0, t) = \sigma_{23}(x_1, x_2, 0, t) = \sigma_{33}(x_1, x_2, 0, t) = 0$ (Case II). At the interface, media 1 and 2 are welded (perfect bounding), i.e., the particle displacement (or the velocity) and the normal traction (vector $\sigma\mathbf{x}_3$) are continuous. The action of sources, that generates the wave motion, is represented, via boundary conditions, by the intro-

duction of volume source densities of force—denoted by $\mathbf{f}$—or of strain rate—denoted by the tensor h; the sources are concentrated at the origin O of the reference frame. The function governing the time dependance of the source (source history) is denoted by $\phi(t)$. The initial condition is that all the layers are at rest for $t \leqslant 0$.

Three types of waves may coexist in an elastic medium: longitudinal or pressure waves (P), transverse or shear waves with vertical (SV) and horizontal (SH) polarizations. Pressure and shear wave speeds are respectively defined by $c_{\mathrm{P}} = \sqrt{(\lambda + 2\mu)/\rho}$ and $c_{\mathrm{S}} = \sqrt{\mu/\rho}$; waves slownesses are defined as $s_{\mathrm{P,S}} = 1/c_{\mathrm{P,S}}$ where P or S must be used for pressure and shear waves, respectively. All through the paper, each time a comma appears between P and S means that the quantities relative to P-waves or S-waves, respectively must be used. In the literature, the P–SV problem and the SH problem are often studied separately (Aki and Richard, 1980). Indeed, in an homogeneous medium, there is no coupling between, on the one hand, P and SV wave motions, and, on the other hand, SH wave motion. In this section, we shall write that the wavefield is the solution of a system of six ordinary differential equations that includes both the P–SV and the SH problems. Formalisms concerned with either the P–SV or the SH problem, respectively deal with systems of four or two equations; the formalism employed here allows to solve P–SV and SH problems together.

2.1.2. Governing equations, boundary and initial conditions

The equation of motion is given by

$$\partial_j \sigma_{ij} - \rho \partial_t v_i = -f_i, \tag{1}$$

where ∂_j and ∂_t denote partial derivatives with respect to x_j and to time, respectively. The term f_i stands for a volume density of body force. The time derivative of Hooke's constitutive law for an elastic isotropic medium including a source of strain rate can take the form

$$\partial_t \sigma_{ij} - \lambda \delta_{ij} \delta_{pq} \partial_p v_q - \mu(\partial_i v_j + \partial_j v_i) = -\lambda \delta_{ij} \delta_{pq} h_{pq} - 2\mu h_{ij}, \tag{2}$$

where δ_{ij} is the Kronecker symbol and h_{ij} is the source of strain rate. Einstein summation convention is used.

2.2. Solution in the transform-domain

In this subsection, we first derive the solution for Cases I and II in a single-medium configuration (the waves never reach the interface with medium 2 so that only the propagation in medium 1 is considered); then the solution in the bimaterial is deduced from the solution in the single-medium configuration.

We use the one-sided Laplace transform with respect to time, and the Fourier transform with respect to the x_1 and x_2 coordinates. For instance, Laplace, Fourier and inverse Fourier transforms successively applied to v_i give

$$\begin{aligned}
\hat{v}_j(\mathbf{x}, p) &= \int_0^\infty \exp(-pt) v_j(\mathbf{x}, t) \mathrm{d}t, \\
\tilde{v}_j(k_1, k_2, x_3, p) &= \int_{-\infty}^{\infty} \int_{-\infty}^{\infty} \exp[ip(k_1 x_1 + k_2 x_2)] \hat{v}_j \mathrm{d}x_1 \mathrm{d}x_2, \\
\hat{v}_j(\mathbf{x}, p) &= (p/2\pi)^2 \int_{-\infty}^{\infty} \int_{-\infty}^{\infty} \exp[-ip(k_1 x_1 + k_2 x_2)] \tilde{v}_j \mathrm{d}k_1 \mathrm{d}k_2,
\end{aligned} \tag{3}$$

where p and pk_j are respectively taken to be the Laplace and Fourier transform parameters.

The Laplace–Fourier transformation of the governing Eqs. (1) and (2), together with the application of the rules concerning the derivatives in the transform-domain, yield a set of equations in which the only

derivatives left are with respect to x_3. Further algebraic manipulations lead to a system of six ordinary differential equations

$$\partial_3 \tilde{\mathbf{b}} = -pA\tilde{\mathbf{b}} + \widetilde{\mathbf{F}}, \tag{4}$$

where $\tilde{\mathbf{b}} = (\tilde{v}_1, \tilde{v}_2, \tilde{v}_3, -\tilde{\sigma}_{13}, -\tilde{\sigma}_{23}, -\tilde{\sigma}_{33})^{\mathrm{T}}$ (here T means transpose) is the unknown vector in the transform domain—called the "motion-stress vector"; its components are continuous across the interface. Matrix A is given in Appendix A. Vector $\widetilde{\mathbf{F}}$ contains the source terms and is defined by

$$\widetilde{\mathbf{F}} = \hat{\phi}(p)\mathbf{X}\delta(x_3), \tag{5}$$

where $\mathbf{X}$ is a vector that depends on the nature of the source and $\hat{\phi}(p)$ is the Laplace transform of the source temporal shape. The Dirac function $\delta(x_3)$ indicates that the source is located at the origin (in the transform domain, $\delta(x_1, x_2, x_3)$ becomes $\delta(x_3)$). Vector $\mathbf{X}$ is defined in the transform domain by the boundary conditions at the source.

The solution of the elastodynamics problem in an unbounded medium will be found in the transform domain as a linear combination of six independent wave motions, corresponding to three upgoing and three downgoing waves of polarizations P, SV and SH. Let D be the matrix of eigenvectors of A and D^{-1} its inverse (see Appendix A). We introduce the vector $\mathbf{w} = D^{-1}\tilde{\mathbf{b}}$; the normalization of D is such that each component of $\mathbf{w}$ is related to the amplitude of the particle velocity of one of the six waves in the transform domain. Multiplication of (4) by D^{-1} leads to

$$\partial_3 \mathbf{w} = -p\Lambda\mathbf{w} + D^{-1}\mathbf{F}, \tag{6}$$

where Λ is a diagonal matrix whose terms, denoted by λ_n (with $n = 1, 6$), are the eigenvalues of A. The homogeneous solution of (6) has the structure of a wave propagating in direction $\mathbf{x}_3$, i.e.,

$$w_n = \text{constant} \times \exp[-p\lambda_n x_3]. \tag{7}$$

The eigenvalues λ_n depend only on the Fourier variables and on one of the slownesses of the medium. The non-zero components of Λ are $\Lambda_{11} = \lambda_1 = -s_3^{-\mathrm{P}}$, $\Lambda_{22} = \lambda_2 = -s_3^{-\mathrm{SV}}$, $\Lambda_{33} = \lambda_3 = -s_3^{-\mathrm{SH}}$, $\Lambda_{44} = \lambda_4 = s_3^{P}$, $\Lambda_{55} = \lambda_5 = s_3^{\mathrm{SV}}$ and $\Lambda_{66} = \lambda_6 = s_3^{\mathrm{SH}}$, where $s_3^{\mathrm{SV}} = s_3^{\mathrm{SH}} = s_3^{S}$; the sign indicates the direction of propagation with respect to x_3 and the superscripts P, SV and SH stand for the three polarizations. The determinantal equation $\det(A - \Lambda) = 0$ yields $s_3^{\mathrm{P,S}} = (s_{\mathrm{P,S}}^2 + k_1^2 + k_2^2)^{1/2}$, where P or S must be used for pressure and shear waves, respectively, ($s_3^{\mathrm{P,S}}$ are sometimes called "vertical slownesses" because they appear in the solution (7) for waves propagating along x_3).

The constant in the solution (7) is determined considering the boundary and initial conditions at the source. The solution for w_n may be rewritten

$$w_n = \hat{\phi}(p) \sum_{k=1}^{6} \left\{ D_{nk}^{-1} X_k \right\} \times \exp[-p\lambda_n x_3]. \tag{8}$$

In what follows, we will use the source term

$$W_n = \sum_{k=1}^{6} \left\{ D_{nk}^{-1} X_k \right\}; \tag{9}$$

upgoing P-waves and SV-waves are associated with W_4 and W_5, respectively, we will use the notations W_{P} and W_{S} for the source terms associated with these waves. From a physical point of view, a source term indicates the amplitude of a wave of a given polarization emitted by the source.

The solution for a component of the motion-stress vector in the transform domain is now

$$\tilde{b}_i = \sum_{n=1}^{6} \{D_{in} w_n\} = \hat{\phi}(p) \times \sum_{n=1}^{6} \{D_{in} W_n \exp[-p\lambda_n x_3]\}. \tag{10}$$

The multiplication by a component of matrix D converts the amplitude of a wave of a given polarization (w_n) in a component of the wave vector $\tilde{b}_i$. In the present study we only make use of the subscripts $n = 4$ and $n = 5$ associated with upgoing P and SV-waves, respectively. From (10), it can be seen that the solution in the transform domain is a sum of six terms corresponding to the six independent waves propagating in an infinite media (upgoing and downgoing P, SV and SH-waves); each term is called a "GR". Let us introduce

$$B_i^n = D_{in} W_n \quad \text{(no summation)}, \tag{11}$$

so that (10) is rewritten

$$\tilde{b}_i = \hat{\phi}(p) \times \sum_{n=1}^{6} \left\{ B_i^n \exp[-p\lambda_n x_3] \right\} = \sum_{n=1}^{6} \tilde{b}_i^n. \tag{12}$$

Each term $\tilde{b}_i^n$ is the contribution to the solution of one of the six GR. The solution in the Laplace domain for a specific GR is finally obtained by applying the inverse Fourier transform

$$\hat{b}_j^n(\mathbf{x}, p) = \hat{\phi}(p) \times (p/2\pi)^2 \int_{-\infty}^{\infty} \int_{-\infty}^{\infty} B_j^n(k_1, k_2) \exp[-p(ik_1 x_1 + ik_2 x_2 + \lambda_n x_3)] \mathrm{d}k_1 \, \mathrm{d}k_2. \tag{13}$$

In fact, $B_j^n(k_1, k_2)$ is a weighting factor indicating the contribution of a specific plane wave—defined through k_1 and k_2—to the solution; integrals of the form of (13) are sometimes called Weyl integrals.

2.2.1. Case I: Solution in the single-medium configuration

This case corresponds to Fig. 1a with $h_1 = \infty$. We take $\mathbf{f} = \mathbf{0}$ (no density of body force) in (1) and $h_{ij} = V_0 \phi(t) \delta_{ij} \delta(x_1, x_2, x_3)$ in (2) (explosion source), where $\delta(x_1, x_2, x_3)$ is the three-dimensional Dirac function and V_0 is the amplitude of the source. The source terms for the buried explosion source are (Van Der Hijden, 1987)

$$W_{\mathrm{P}} = V_0 \frac{s_{\mathrm{P}}}{2 s_3^{\mathrm{P}}} \left(\frac{3\lambda + 2\mu}{\lambda + 2\mu} \right), \qquad W_{\mathrm{S}} = 0. \tag{14}$$

The solution for a component of the motion-stress vector in the Laplace domain is then

$$\hat{b}_j(\mathbf{x}, p) = \hat{b}_j^4(\mathbf{x}, p), \tag{15}$$

with $W_4 = W_{\mathrm{P}}$.

2.2.2. Case II: Solution in the single-medium configuration

This case corresponds to Fig. 1b with $h_1 = \infty$. We take $\mathbf{f} = \mathbf{0}$ in (1) and $h_{ij} = 0$ in (2). In addition to (1) and (2), the boundary conditions at the free surface (defined by $x_3 = 0$) require

$$\begin{aligned} &\sigma_{33}(x_1, x_2, 0, t) = f_0 \phi(t) \delta(x_1, x_2), \\ &\sigma_{13}(x_1, x_2, 0, t) = \sigma_{23}(x_1, x_2, 0, t) = 0, \end{aligned} \tag{16}$$

where $\delta(x_1, x_2)$ is the two-dimensional Dirac function and f_0 is the amplitude of the force source. Some algebraic manipulations yield the source terms for the force at the free surface in direction x_3

$$W_{\mathrm{P}} = f_0 \frac{\chi}{2\mu c_{\mathrm{P}} (s_3^{\mathrm{P}} s_3^{\mathrm{S}} S^2 + \chi^2)}, \quad W_{\mathrm{S}} = f_0 \frac{s_3^{\mathrm{P}} S}{2\mu c_{\mathrm{S}} (s_3^{\mathrm{P}} s_3^{\mathrm{S}} S^2 + \chi^2)}, \tag{17}$$

where $S^2 = -k_1^2 - k_2^2$ and $\chi = 0.5s_S^2 - S^2$. The solution for a component of the motion-stress vector in the Laplace domain is then

$$\hat{b}_j(\mathbf{x}, p) = \hat{b}_j^4(\mathbf{x}, p) + \hat{b}_j^5(\mathbf{x}, p), \tag{18}$$

with $W_4 = W_P$ and $W_5 = W_S$.

The source terms for the buried force source may be found in Van Der Hijden (1987, p. 58). It is to note that for the sources considered in this paper, only P and SV waves are generated.

2.2.3. Solution for a bimaterial

In the transform-domain, the solution of the problem in a bimaterial is deduced from the solution (8) for the single-medium configuration. Many authors have shown with different formalisms (see Spencer, 1960; Aki and Richard, 1980; Kennett, 1983; Van Der Hijden, 1987) that the interaction of waves with interfaces can be accounted for by multiplying w_n by specific terms called "generalized transmission and reflection coefficients". Reflection and transmission coefficients can be computed numerically following a procedure involving matrices D and D^{-1} (Van Der Hijden, 1987) or, alternatively, their analytical expressions may be implemented. Since we will derive an analytical solution in Section 4, we need analytical expressions for the coefficients; the well-known transmission and reflection coefficients for plane waves (see Spencer, 1960; Aki and Richard, 1980, p. 144) are used here: to take the interfaces into account, we simply have to multiply each plane wave appearing in the Weyl integral (13) by the corresponding reflection or transmission coefficients; these depend on k_1 and k_2, which determine the incidence of a plane wave in the Weyl integral. We are interested in the transmission of waves from medium 1 to 2, thus the coefficients needed are

$$\begin{aligned} T_{P\to P}(S) &= 2\rho_1 s_3^{P;1}\frac{Fc_{P;1}}{Dc_{P;2}}; \quad T_{P\to S}(S) = -2\rho_1 s_3^{P;1}\frac{HSc_{P;1}}{Dc_{S;2}}; \\ T_{S\to P}(S) &= 2\rho_1 s_3^{S;1}\frac{GSc_{S;1}}{Dc_{P;2}}; \quad T_{S\to S}(S) = 2\rho_1 s_3^{S;1}\frac{Ec_{S;1}}{Dc_{S;2}}, \end{aligned} \tag{19}$$

where $T_{\alpha\to\beta}$ ($\alpha = P, S$; $\beta = P, S$) is the transmission coefficient corresponding to the wave with polarization α generated by the source in medium 1 and transmitted in medium 2 with the polarization β; subscripts and superscripts 1 and 2 stand for a medium, and

$$\begin{aligned} a &= \rho_2(1 - 2c_{S;2}^2S^2) - \rho_1(1 - 2c_{S;1}^2S^2); \quad b = \rho_2(1 - 2c_{S;2}^2S^2) + 2\rho_1 c_{S;1}^2S^2; \\ c &= \rho_1(1 - 2c_{S;1}^2S^2) + 2\rho_2 c_{S;2}^2S^2; \quad d = 2(\rho_2 c_{S;2}^2 - \rho_1 c_{S;1}^2); \\ E &= bs_3^{P;1} + cs_3^{P;2}; \quad F = bs_3^{S;1} + cs_3^{S;2}; \\ G &= a - ds_3^{P;1}s_3^{S;2}; \quad H = a - ds_3^{P;2}s_3^{S;1}; \\ D &= EF + GHS^2. \end{aligned} \tag{20}$$

Aside from the introduction of the transmission coefficient, the phase term $\lambda_n x_3$ appearing in (13) is split into two parts: it is replaced by $s_3^{\alpha;1}h_1 + s_3^{\beta;2}h_2$, where h_1 and h_2 are the distances along x_3 traveled by the wave, and α and β indicate the polarization (P- or S-wave) in media 1 and 2. Eventually, (13) becomes

$$\hat{b}_j^{\alpha\to\beta}(\mathbf{x}, p) = \hat{\phi}(p) \times \left(\frac{p}{2\pi}\right)^2 \int_{-\infty}^{\infty}\int_{-\infty}^{\infty} B_j^{\alpha\to\beta}(k_1, k_2) T_{\alpha\to\beta} \exp[-p(ik_1x_1 + ik_2x_2 + s_3^{\alpha;1}h_1 + s_3^{\beta;2}h_2)]\mathrm{d}k_1\,\mathrm{d}k_2, \tag{21}$$

where the symbol $\alpha \to \beta$ designates the GR corresponding to the wave with polarization α generated by the source in medium 1 and transmitted in medium 2 with the polarization β; and from (11), we rewrite B_i^n

$$B_i^{\alpha\to\beta}(k_1, k_2) = D_{im}^{(2)} W_l^{(1)}, \tag{22}$$

where superscripts (1) and (2) stand for the medium in which the quantities are evaluated. Subscript l and m are associated with polarizations α and β, respectively; in the present paper, l and m take the values 4 and 5 depending on the GR under study; for example, the ray denoted by $P \to S$ is associated with $l = 4$ and $m = 5$.

The total wave-field is the sum of all the possible GRs; for the explosion source and the vertical force source, respectively two and four GRs must be computed.

2.2.3.1. Case I: Solution in the bimaterial. The solution in medium 2 for a component of the motion-stress vector in the Laplace domain is

$$\hat{b}_j(\mathbf{x},p) = \hat{b}_j^{P\to P}(\mathbf{x},p) + \hat{b}_j^{P\to S}(\mathbf{x},p). \tag{23}$$

2.2.3.2. Case II: Solution in the bimaterial. In this case, the configuration includes a free surface; thus, multiple reflections occur in medium 1 between the free surface and the interface with medium 2. These reflections are not taken into account in this study, however, the solution including multiple reflections may be obtained by adding the corresponding terms to the solution presented. The solution in medium 2 for a component of the motion-stress vector in the Laplace domain is

$$\hat{b}_j(\mathbf{x},p) = \hat{b}_j^{P\to P}(\mathbf{x},p) + \hat{b}_j^{P\to S}(\mathbf{x},p) + \hat{b}_j^{S\to P}(\mathbf{x},p) + \hat{b}_j^{S\to S}(\mathbf{x},p). \tag{24}$$

In the remainder of this section, we will describe the method used to transform each GR contribution (21) in the Laplace-transform domain back to the space–time domain by using the CdH method.

2.3. Transformation back to the space–time domain

Let us perform the first standard substitution of the three-dimensional CdH method.

$$ik_1 = s\cos\theta - iq\sin\theta, \quad ik_2 = s\sin\theta + iq\cos\theta, \tag{25}$$

where q is a real number and s can be a complex number. Variables θ and r ($0 \leqslant \theta \leqslant 2\pi$, $0 \leqslant r < \infty$) are the polar coordinates in the (x_1, x_2) plane

$$x_1 = r\cos\theta, \quad x_2 = r\sin\theta. \tag{26}$$

The vertical slownesses are now given by

$$s_3^{P,S;m} = (s_{P,S;m}^2 - s^2 + q^2)^{1/2}, \tag{27}$$

where m stands for the number—1 or 2—of the medium. Noting that $ik_1x_1 + ik_2x_2 = sr$, (21) is rewritten

$$\hat{b}_j^{\alpha\to\beta}(\mathbf{x},p) = \hat{\phi}(p) \times (p^2/4i\pi^2) \int_{-\infty}^{\infty} \mathrm{d}q \int_{-i\infty}^{i\infty} B_j^{\alpha\to\beta}(s,q) T_{\alpha\to\beta} \exp[-p(sr + s_3^{\alpha;1}h_1 + s_3^{\beta;2}h_2)]\mathrm{d}s. \tag{28}$$

In (28), the integration over the variable s lies along the imaginary axis. The CdH method consists of a deformation of the contour of integration away from the imaginary axis; this requires to extend the definition of the integrand in the complex s plane by analytic continuation. This cannot be achieved without a detailed analysis of the analyticity of the integrand (for a detailed discussion see Van Der Hijden, 1987). In essence, the singularities of $B_j^{\alpha\to\beta}(s,q)$ in the complex s plane must be identified: they are found to be the values of s canceling $s_3^{P,S;m}$ (these values are always real). If during its deformation (from the imaginary axis to a curve in the complex s plane), the contour crosses a singularity, another integral corresponding to a head wave must be evaluated by using residue theorems. Whether or not this happens depends on both the

location of the receiver with respect to the source and on the material constants; in the numerical examples presented in this paper the contour does not cross any singularity during its deformation—this is mainly because we will only be interested in solutions around the $\mathbf{x}_3$-axis.

The next step of the method is to take τ to be the real variable—with the dimension of time—defined by

$$\tau = sr + s_3^{\alpha;1} h_1 + s_3^{\beta;2} h_2. \tag{29}$$

The solution of this equation for $s(\tau)$ is the CdH contour for the GR under consideration. Considering the symmetry properties of both $B_j^{\alpha\to\beta}(s,q)$ and the contour, (28) can be rewritten as an integral over τ

$$\hat{b}_i^{\alpha\to\beta}(\mathbf{x},p) = \hat{\phi}(p) \times (p^2/2\pi^2) \int_{-\infty}^{\infty} \mathrm{d}q \int_{T(q)}^{\infty} \Im[B_i^{\alpha\to\beta}(s,q) T_{\alpha\to\beta}(s,q) \partial_\tau s] \exp[-p\tau] \mathrm{d}\tau, \tag{30}$$

where $\Im$ denotes the imaginary part and $T(q)$ is the minimum of τ on the contour; it corresponds to the point at which the contour intersects the real axis and is given by (Van Der Hijden, 1987)

$$T(q) = \frac{(s_{\alpha;1}^2 + q^2)^{1/2} h_1}{\cos \Theta_1(q)} + \frac{(s_{\beta;2}^2 + q^2)^{1/2} h_2}{\cos \Theta_2(q)}, \tag{31}$$

where the $\Theta_i(q)$ may be compared to the angles of geometrical rays with respect to the interface, obtained following Snell's law; $T(q)$ can be thought of as a the travel time from the source to the receiver of a wave traveling with slownesses $(s_{\alpha;1}^2 + q^2)^{1/2}$ and $(s_{\beta;2}^2 + q^2)^{1/2}$ in media 1 and 2, respectively. The angles $\Theta_i(q)$ are defined through the two equations

$$(s_{\alpha;1}^2 + q^2)^{1/2} \sin \Theta_1(q) = (s_{\beta;2}^2 + q^2)^{1/2} \sin \Theta_2(q) = s^0(q), \tag{32}$$

and

$$r = h_1 \tan \Theta_1(q) + h_2 \tan \Theta_2(q), \tag{33}$$

where $s^0(q)$ is the horizontal slowness given by the intersection of the CdH contour with the real axis; Eq. (32) is the equivalent of Snell's law and (33) is the horizontal distance traveled by a wave. Next, the order of integration in (30) must be changed, i.e., the integration over q must be performed first. The new limits of integration are $-Q(\tau)$ and $Q(\tau)$; they are solutions for q of the equation $\tau = T(q)$, where $T(q)$ is defined by (31). After changing the order of integration, we get

$$\hat{b}_i^{\alpha\to\beta}(\mathbf{x},p) = \hat{\phi}(p) \times (p^2/2\pi^2) \int_{T_a}^{\infty} \left\{ \int_{-Q(\tau)}^{Q(\tau)} \Im[B_i^{\alpha\to\beta}(s,q) T_{\alpha\to\beta}(s,q) \partial_\tau s] \mathrm{d}q \right\} \exp[-p\tau] \mathrm{d}\tau, \tag{34}$$

where $T_\mathrm{a} = T(q=0)$ appears to be the arrival time of the wave.

Through the steps of the CdH method, the double integration over k_1 and k_2 has been changed to an integration of a real quantity over the real variable q and an integration over the time variable τ. In (34), the integration over τ has the form of a forward Laplace transform, the transformation back to the time domain can thus be done by inspection. Finally, noting that the expression (34) is a product in the Laplace domain, the solution for one of the components of the motion-stress vector is the convolution (denoted by $*$) of a source term by the Green's function of the problem

$$\begin{cases} b_j^{\alpha\to\beta}(\mathbf{x},t) = 0 \quad \text{for } 0 \leqslant t \leqslant T_\mathrm{a} \\ b_j^{\alpha\to\beta}(\mathbf{x},t) = (1/2\pi^2) \partial_{tt} \phi(t) \ * \ \int_{-Q(t)}^{Q(t)} \Im[B_j^{\alpha\to\beta}(s,q) T_{\alpha\to\beta}(s,q) \partial_t s] \mathrm{d}q \quad \text{for } T_\mathrm{a} < t \end{cases} \tag{35}$$

It is to note that for the source time function $\phi(t) = H(t)$, where $H(t)$ is the Heaviside step function, the displacement in the medium is given by $(u_1, u_2, u_3) = (b_1, b_2, b_3)$, and no convolution is required.

2.4. Energy flux and strain energy

In this section, we show how an approximation to the strain energy carried by the wave can be readily obtained from the components of vector **b**. Let $E = \int_V (E_d + K)\mathrm{d}V$ be the total energy carried by the wave in a disturbed region of volume V, $\mathrm{d}V$ being the associated differential element; E_d and K are respectively the volumic strain and kinetic energies. The energy flux vector (Poynting vector), denoted by **P** is defined by (Nayfeh and Payfeh, 1995),

$$\partial_t E = -\int_S \mathbf{P}.\mathbf{n}\mathrm{d}S, \quad \text{with } \mathbf{P} = -\sigma\mathbf{v}, \tag{36}$$

where S stands for the surface of the disturbed region, $\mathrm{d}S$ is its associated differential element, and **n** stands for the unit outer normal vector to S. The volume density of total energy is denoted by E_v. The components of the motion stress vector **b** are used to evaluate $P_3 = v_1\sigma_{13} + v_2\sigma_{23} + v_3\sigma_{33}$ which is the projection of **P** in direction $\mathbf{x}_3$. All the components of **P** can be derived from P_3 if the normal direction to the wave front—direction of **P** in an isotropic medium—is known; this direction might be computed through the equations yielding the wave front (31) and (33).

Without loss of generality, we consider the general equation for the particle displacement, denoted by u_i, induced by a longitudinal plane wave of unit—and constant—amplitude propagating in direction $\mathbf{x}_3$ with wave speed c_P

$$(u_1, u_2, u_3) = (0, 0, f(x_3 - c_\mathrm{P}t)); \tag{37}$$

and the particle displacement, induced by a shear plane wave, in the plane $(\mathbf{x}_1, \mathbf{x}_2)$, of unit—and constant—amplitude propagating in direction $\mathbf{x}_3$ with wave speed c_S

$$(u_1, u_2, u_3) = (f(x_3 - c_\mathrm{S}t), 0, 0). \tag{38}$$

The densities of strain energy associated with these waves are

$$\begin{aligned} E_d^\mathrm{P} &= \frac{1}{2}\sigma_{33}\partial_3 u_3 = \frac{1}{2}(\lambda + 2\mu)(\partial_3 u_3)^2 = \frac{1}{2}\rho c_\mathrm{P}^2 (f'(x_3 - c_\mathrm{P}t))^2, \\ E_d^\mathrm{S} &= \frac{1}{2}\sigma_{13}\partial_3 u_1 = \frac{1}{2}\rho c_\mathrm{S}^2 (f'(x_3 - c_\mathrm{S}t))^2, \end{aligned} \tag{39}$$

and the densities of kinetic energy are

$$K^{\mathrm{P,S}} = \frac{1}{2}\rho c_{\mathrm{P,S}}^2 (f'(x_3 - c_{\mathrm{P,S}}t))^2. \tag{40}$$

Therefore, the volume density of total energy ($E_v^{\mathrm{P,S}} = E_d^{\mathrm{P,S}} + K^{\mathrm{P,S}}$), carried by a longitudinal or a shear plane wave, is for one half strain energy and for the other half kinetic energy: $E_d^{\mathrm{P,S}} = K^{\mathrm{P,S}} = (1/2)E_v^{\mathrm{P,S}}$.

Let us evaluate $\partial_t E$ in (36), for the plane wave propagating in direction x_3, on the surface of a parallelepiped whose faces are parallel to the axes of the Cartesian frame; since **P** is along $\mathbf{x}_3$, the only contributions to the integral are on the two surfaces normal to $\mathbf{x}_3$. Eq. (36) yields

$$-\partial_t E = \left[P_3(x_1, x_2, x_3^+, t) - P_3(x_1, x_2, x_3^-, t)\right] \times A_3, \tag{41}$$

where A_3 is the area of a face, x_3^+ and x_3^- are the coordinates along $\mathbf{x}_3$ of the faces normal to $\mathbf{x}_3$. Let $\Delta x_3 = x_3^+ - x_3^-$ be the height of the parallelepiped. Its volume is $A_3\Delta x_3$. Letting Δx_3 go to zero, $-\partial_t E(A_3\Delta x_3)^{-1} = \left[P_3(x_1, x_2, x_3^+, t) - P_3(x_1, x_2, x_3^-, t)\right](\Delta x_3)^{-1}$ reduces to

$$-\partial_t E_v = \partial_3 P_3(x_1, x_2, x_3, t). \tag{42}$$

The Poynting vector calculated for a plane wave is a solution of the one-dimensional wave equation, that is,

$$\partial_3 P_3^{\mathrm{P,S}} = -\frac{1}{c_{\mathrm{P,S}}}\partial_t P_3^{\mathrm{P,S}}. \tag{43}$$

Introducing (43) in (42) yields, after integration, the relations between the volume density of strain energy and the Poynting vector for P and S plane waves:

$$E_d^{\mathrm{P,S}}(x_1,x_2,x_3,t) = \frac{1}{2c_{\mathrm{P,S}}} P_3^{\mathrm{P,S}}(x_1,x_2,x_3,t) + \text{constant}, \tag{44}$$

where the constant is zero if the medium is at rest before the arrival of the wave. Eqs. (44) are valid for a plane wave, i.e., waves whose amplitude are independent of x_1 and x_2 and whose front is a plane (here, the plane (x_1,x_2)); (44) is also valid in an approximate way for any wave whose amplitude varies slowly with respect to x_1 and x_2 and which wave front has a weak curvature. This is of importance in the numerical examples presented in this paper: waves in medium 2 will satisfy the aforementioned conditions so that the Poynting vector yields an approximation of the strain energy carried by the waves.

3. An analytical solution

The developments given in Section 2 can be used to compute the exact three-dimensional wave field generated by a point source in a bimaterial. In most cases, the solution cannot be found without the help of numerical techniques; in particular, the CdH contour (29), the limits of integration, given by the Eqs. (31)–(33), and the integration over q cannot be obtained analytically. In this section, we show that for an axisymmetric source (with respect to the $\mathbf{x}_3$-axis), and a receiver located on the $\mathbf{x}_3$-axis, an analytical solution can be derived. We note that in this case, due to symmetry, $v_1 = v_2 = 0$, hence $P_3 = v_3\sigma_{33}$.

A useful variable: It appears that, with the aforementioned conditions, all the terms in (35) only depend on the variable $S^2 = s^2 - q^2$; the limits of integration $\pm Q(\tau)$ and the transmission coefficients can be written as a function of S too. With the notation used above $k_1^2 + k_2^2 = -S^2$, thus a value of S corresponds to the incidence of a particular plane wave in the decomposition (21). The new variable S appears to be the natural variable for the study of the axisymmetric case.

Cagniard-de Hoop contour: The equation of the CdH contour now can be solved analytically; using

$$s(q,t) = \pm\sqrt{q^2 + S^2(t)}. \tag{45}$$

For $r = 0$, Eq. (29) for the CdH contour $s(q,t)$ becomes

$$t = h_1\sqrt{s_{\alpha;1}^2 - S^2} + h_2\sqrt{s_{\beta;2}^2 - S^2}. \tag{46}$$

From (46) it is obvious that S is a function of t only (for a given receiver position h_1, h_2, and a given bimaterial with slownesses $s_{\alpha;1}$ and $s_{\beta;2}$). Using the change of variables $X = (s_{\alpha;1}^2 - S^2)^{1/2}$ and $Y = (s_{\beta;2}^2 - S^2)^{1/2}$, related by $X^2 - Y^2 = s_{\alpha;1}^2 - s_{\beta;2}^2$, Eq. (46) can be solved exactly for S (this is impossible if $r \neq 0$). We introduce the arrival time of the wave $T_{\mathrm{a}} = h_1 s_{\alpha;1} + h_2 s_{\beta;2}$.

For the particular case where $h_1 = h_2 = h$ the solution for Y is

$$Y = [2h^2 s_{\beta;2}(s_{\alpha;1} + s_{\beta;2}) + t^2 - T_{\mathrm{a}}^2](2th)^{-1}. \tag{47}$$

If $h_1 \neq h_2$ then Y satisfies a quadratic equation whose solutions are

$$Y = \frac{th_2 - h_1^2\sqrt{\Delta}}{h_2^2 - h_1^2}, \quad \text{where } \Delta = h_1^{-2}\left[(h_1 s_{\beta;2} + h_2 s_{\alpha;1})^2 - T_{\mathrm{a}}^2 + t^2\right]. \tag{48}$$

We note that $\Delta > 0$ for $t > T_a$, thus Y is always real. Finally,

$$S = \pm\sqrt{s_{\beta;2}^2 - Y^2}. \tag{49}$$

We also have

$$\partial_t s(q,t) = \pm\frac{S\partial_t S}{\sqrt{q^2 + S^2(t)}}, \quad \text{where } S\partial_t S = \mp Y\partial_t Y. \tag{50}$$

Integration over q: The limits of the integral appearing in (35) are obtained in closed form using the same procedure as for the derivation of the contour. Considering (33), it is obvious that $\Theta_1 = \Theta_2 = 0$ for $r = 0$; then the equation for $T(q)$ (31) is rewritten

$$T(q) = h_1\sqrt{s_{\alpha;1}^2 + q^2} + h_2\sqrt{s_{\beta;2}^2 + q^2}. \tag{51}$$

Comparing (46) and (51), it appears that the solution for $-q^2$ in (51) is the solution for S^2 in (46). It follows that once S has been calculated, $Q(\tau)$ is given by $Q(\tau) = iS(\tau)$. Furthermore, for an axisymmetric source, the integrand in (35) only depends on $S(\tau)$, except for a term arising from $\partial_\tau s$; the integral to be evaluated reduces to

$$\int_{-Q(\tau)}^{Q(\tau)} \frac{\mathrm{d}q}{\sqrt{q^2 + S^2(\tau)}} = 2 \times \frac{Q(\tau)}{\sqrt{S^2(\tau)}} \times \arcsin(1) = -i\pi, \tag{52}$$

where we have used the following result:

$$\arcsin z = \int_0^z \frac{\mathrm{d}t}{(1-t^2)^{1/2}}.$$

Solution: Finally, for an axisymmetric source, and in the case $r = 0$, the solution of the elastodynamics problem in the bimaterial (35) is rewritten

$$b_i^{\alpha\to\beta}(x_3,t) = -\frac{1}{2\pi}\partial_{tt}\phi(t) \;*\; \Re e[B_i^{\alpha\to\beta}(S)T_{\alpha\to\beta}(S)S\partial_t S]. \tag{53}$$

The analytical solution (53) gives insight into the physical response of a bimaterial; this will be discussed in another paper. For the present paper, the analytical solution was used to check and optimize the computation scheme yielding the response of the bimaterial in the general case (Eq. (35)). It is to note that the wave field in medium 1 (incident and reflected waves) for a source and a receiver on the $\mathbf{x}_3$-axis can be obtained in a similar way, using appropriate reflection coefficients.

For more than one interaction with an interface, the solution on the $\mathbf{x}_3$-axis cannot be obtained in closed form; however, the expression (35) takes a simple form, very similar to (53). For $n-1$ interactions with interfaces, the equation giving the CdH contour is rewritten for the variable S

$$t = \sum_{i=1}^{n} h_i\sqrt{s_{\mathrm{P,S};i}^2 - S^2}. \tag{54}$$

where h_i and $s_{P,S;i}$ are respectively the thickness and the wave slowness in medium i. The solutions for s and $\partial_t s$ are still given by

$$s(q,t) = \pm\sqrt{q^2 + S^2(t)}, \quad \partial_t s(q,t) = \pm\frac{S\partial_t S}{\sqrt{q^2 + S^2(t)}}. \tag{55}$$

The solution S must be computed by numerical methods (for instance, with a Newton–Raphson scheme). Fortunately, S is still a constant for a given t (independent of q) and the integral in (35) can be evaluated in

the same manner as for the bimaterial. Let $\Pi_r(S)$ be the product of all the reflection and transmission coefficients required to calculate the response due to a given GR, the solution takes the form

$$b_i^{\alpha\to\beta}(x_3,t) = -\frac{1}{2\pi}\partial_{tt}\phi(t) \;*\; \Re e[B_i^{\alpha\to\beta}(S)\Pi_r(S)S\partial_t S], \tag{56}$$

where $B_i^{\alpha\to\beta}(S) = D_{im}^{(n)}W_l^{(1)}$ (see Eq. (22)) is the product of a coupling term evaluated in the medium of the receiver and a source term evaluated in the medium of the source.

The major simplification from the equations displayed by Van Der Hijden (1987) in the general case is the elimination of the numerical integration over q. Furthermore, since in most axisymmetric problems, the energy maximum is located on the $\mathbf{x}_3$-axis, our solutions yield the energy maxima in the (x_1, x_2) plane; this should find applications, in the traditional mechanical fields concerned with transient wave propagation in layered media.

4. Computational scheme

The evaluation of (35) is split into two parts

- Computation of the integral over q that will thereafter be referred to as the Green's function.
- Evaluation of the response to a physical excitation by convolution with the second derivative of a pulse history. We note that $\phi(t)$ must be a twice continuously derivable function, thus it is worth having an analytical expression for $\phi(t)$ so that it can be derived in closed form.

Most of the numerical solutions obtained with the CdH method are based on asymptotic approximations of (35) (Kennett, 1983) (Herrmann, 2001); this allows the elimination of the integration, very much like for two-dimensional cases. These approximations are valid at high frequencies or far from the source; since we were interested in solutions close to the source, we have developed a numerical scheme following the method described in Section 2 and giving the exact Green's function—including near-field terms—of the elastodynamics problem. Procedures specific to the method are: (i) the numerical evaluation of the CdH contour; (ii) the computation of the waves arrival times; (iii) the computation of the integration limits, i.e., $Q(t)$; (iv) the numerical integration over q. The procedure presented here for a bimaterial can be extended to any number of interactions with interfaces. The integrand appearing in (28) has singularities in the complex s plane. Then, if during the deformation of the contour from the imaginary axis to the curve defined by (29), those singularities are crossed, one must implement an additional numerical procedure to evaluate the integrand at the singularities, yielding a head wave contribution. A way to test the presence or the absence of head waves is to check whether or not there exists a value $S_{\mathrm{P,S};m} = (s_{\mathrm{P,S};m}^2 + q^2)^{1/2}$ inferior to $s^0(q)$ (see Eq. (32)). We have checked that the numerical examples presented here do not involve any contribution of a singularity (no head waves). However, if the receiver is located close to the interface and at a sufficiently large radial distance, a head wave may appear.

Green's functions are computed for t in ranges $[T_\mathrm{a}; T_{\max}]$, where T_a is the arrival time of the GR—computed using both (31)–(33); the value of $T_{\max}$ depends on the time window one is interested in.

If the two media are weakly coupled (wave speeds in the two media are very different), some specific problems arise. In particular, the procedure used by Van Der Hijden (1987) to compute the transmission coefficients from matrices D and D^{-1} should not be used: it includes a numerical inversion of a matrix which is ill-conditioned (Issacson and Keller, 1966) for weakly coupled media; the closed form expressions for the transmission coefficients should be used here.

The limits of integration: For each t, an integration in the range $[-Q(t); Q(t)]$ must be performed (see Eq. (35)), where $Q(t)$ is solution of $T(q) = t$ given by (31). This equation is solved with the Newton–Raphson

method. For each iteration, the angles $\Theta_i(q)$ are computed using both (32) and (33): let subscript n denote the media associated with the smallest slowness appearing in (29); using Snell's law (32), we write $\Theta_m(q)$ $(m \neq n)$ in function of $\Theta_n(q)$; substitution in (33) leads to

$$0 = r - h_m \tan\left(\arcsin\frac{S_n(q)\sin\Theta_n(q)}{S_m(q)}\right) - h_n \tan\Theta_n(q), \tag{57}$$

where $S_k = (s^2_{\mathrm{P,S};k} + q^2)^{1/2}$ $(k = n, m)$; (57) is solved by using a dichotomy method. It is necessary to use n associated with the smallest slowness to keep $S_n(q) < S_m(q)$ so that the function arcsin can be evaluated. The derivatives in the Raphson–Newton iterations are obtained with a finite difference scheme.

The CdH contour: The complex variable s is found for each (t, q) by solving (29) with the Newton–Raphson method. The method requires an initial value to be supplied; numerical tests have shown that this value must be both a real number and close to zero to guarantee convergence. The term $\partial_\tau s$ appearing in (35) can be written as a function of s using the definition of the contour:

$$\partial_\tau s = \left(r - \frac{sh_1}{s_3^{\alpha;1}} - \frac{sh_2}{s_3^{\beta;2}}\right)^{-1}. \tag{58}$$

Numerical integration over q: The integration over q (see Eq. (35)) is carried out numerically by using the trapezoidal rule. The discretization must be done for each t since the integration range is not constant. The integrand contains a singularity (associated with the term $\partial_t s(t, q)$) at each integration limit; although they are integrable singularities, they can lead to numerical problems. We have used a couple of transformations for the variable q, adapted from Johnson (1974), to avoid numerical problems. The integral over the intervals $[-Q(t); Q(t)]$ is split into two integrals over $[-Q(t); 0]$ and $[0; Q(t)]$; then a new variable of integration, denoted by v, is defined as $q = v^2 - Q(t)$ and $q = Q(t) - v^2$, respectively in each interval.

Computation of the physical response: If the contributions from the different GRs are well separated in time, the physical response might be computed for each ray separately; however in the general case the sum of the contribution should be performed first. For the source time function we used a four-point optimum Blackman window (Fig. 2) (Van Der Hijden, 1987); its second derivative is given by

$$\partial_{tt}\phi(t) = \begin{cases} 0 & \text{when} \quad -\infty < t \leqslant 0, \\ -\sum_{n=0}^{3} b_n n^2 \cos(2\pi n t/T) & \text{when} \quad 0 < t < T, \\ 0 & \text{when} \quad T \leqslant t < \infty \end{cases} \tag{59}$$

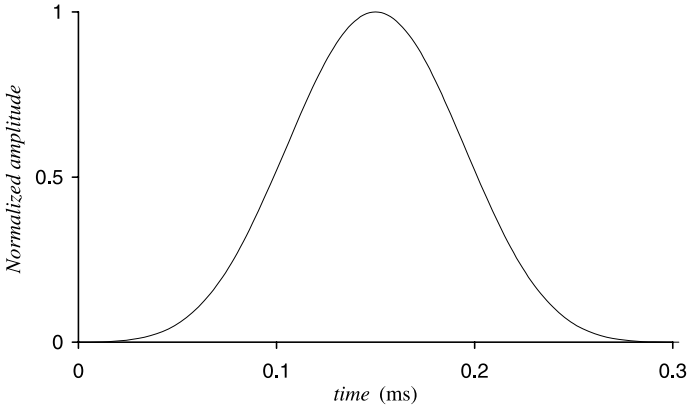

Fig. 2. Normalized time pulse shape $\phi(t)$ used in the computation.

in which the constants b_n are given by $b_0 = 0.35869$, $b_1 = -0.48829$, $b_2 = 0.14128$ and $b_3 = -0.01168$; T is the duration of the pulse. The convolution is carried out numerically with the trapezoidal rule.

Program verification: We have performed calculations in simplified cases in order to test the numerical procedures. For the explosion source, we have reproduced the analytical solutions (see Love, 1927; Eringen and Suhubi, 1975) available for a homogeneous medium (in our program adapted to a bimaterial, the properties of the two media were set to the same values, yielding transmission coefficients equal to one); Green's functions plotted according to the analytical solutions and obtained with our program were indistinguishable. Secondly, thanks to the analytical solution obtained on the $\mathbf{x}_3$-axis (see Section 4), we were able to evaluate the numerical scheme at particular locations in the case of two different media. This tested the efficiency of the contour determination procedure, the efficiency of the numerical integration over q and it also validated the procedure for the computation of the transmission coefficient. For a force source at the free surface, we could compare our solution to that given by Johnson (1974) for a semi-infinite medium; furthermore, taking $\partial_t \phi(t) = \delta(t)$ we reproduced—some time after the arrival of the wave—the classical static solution for a semi-infinite medium subjected to a vertical point force. Finally, we have compared normalized results for a bimaterial, for a set of radial distances, to those of another scheme (Herrmann, 2001); the results obtained with our program agreed those calculated by Herrmann's program.

5. Numerical examples: wave propagation in a model of the thorax

In the present section, we use the solutions of the elastodynamics problem for the bimaterial exhibited in Sections 2 and 3 together with the numerical scheme described in Section 4 to gain insights into the phenomena associated with a high velocity impact (projectile velocity about 500 m s^{-1}) on the thorax: we study the distribution of energy in a model of the thorax due to the stress waves generated at the impact point. More precisely, we highlight some particularities of the distribution of energy in a medium representing the lung. The time history of the loading of the thorax is modeled by a Blackman window (Fig. 2), defined by (59); all the results presented in this section have been obtained with a pulse duration $T = 0.3 \times 10^{-3}$ s. Two cases are investigated. The configuration of Case I consists of two homogeneous semi-infinite media, media 1 and 2, standing for the thoracic wall and for the lung, respectively (Fig. 1a); in this case, a buried explosion source placed in medium 1 at 2 cm below the interface generates the wave motion. In Case II, medium 1 is bounded by a free surface at $x_3 = 0$ (Fig. 1b); in this case, a point force in direction x_3 generates the wave motion at the free surface. The explosion source only generates a P-wave in medium 1, thus receivers in medium 2 are reached by two GRs (see Eq. (23)): ray PP is the part of the incident energy transmitted as a P-wave and ray PS is the part of the incident energy transmitted as a S-wave; the force source generates both a P-wave and a S-wave in medium 1, thus receivers in medium 2 are reached by four GRs (see Eq. (24)): PP and SS preserve the initial polarization and PS and SP are created upon conversion at the interface. We give to medium 1 the mechanical properties of muscle (Yang and Wang, 1998); the properties of medium 2 are discussed in the next subsection.

5.1. On the lung model

The lung can be thought of as a biphasic material: a multitude of air sacs separated by thin soft tissue walls. However, for the length and time scales of this study, the lung can be modeled as a homogeneous, isotropic material. This hypothesis has been made by several authors and has been validated by experiments (Jahed et al., 1989). As a consequence of the biphasic structure, the P-waves and S-waves speeds in the lung are very low; experimental data give P-wave speeds between 6 and 30 m s^{-1}, measured S-wave speeds are about three times less than the P-wave speeds (Jahed et al., 1989). In order to test the influence of the

mechanical properties chosen for the lung on the repartition of energy, we investigate the response for different lung's mechanical properties. The properties of medium 1 (thoracic wall) are kept constant while the properties of medium 2 (lung) vary. These properties are collected in Table 1. "Soft Lung", "Hard Lung 1" and "Hard Lung 2" are relatively "soft" materials for which wave speeds are consistent with experimental data. "Homogeneous medium" indicates that media 1 and 2 have the same mechanical properties; this case describes a lung as 'hard' as the thoracic wall, it is not realistic, but highlights the phenomena induced by weak acoustic coupling.

The analytical solution derived in Section 3 has been used to compute the x_3-component of the Poynting vector—denoted by $P_3(t)$—in medium 2, i.e., the transient energy flux in direction x_3. Results are presented, for the four pairs of media of Table 1 and in Case I (explosion source). In Fig. 3, we plot normalized maxima of $P_3(t)$ for the four pairs of media (typical plots of $P_3(t)$ for the "Soft Lung" model are represented in Fig. 4 and commented in the next section). Using the equation of the arrival time (31) at a given receiver, some P-wave fronts—at a given time—for the different lung models are plotted in Fig. 5; the shape of S-wave fronts (not represented) are similar to the shape of the P-waves fronts.

The decrease in amplitude for each pair of media (Fig. 3) is due to geometrical spreading; therefore, the decrease is all the more important as the front's curvature (see Fig. 5) is large. Obviously, the front for the homogeneous case is spherical; in contrast, wave fronts for the three lung models are almost plane and there

Table 1
Lamé's coefficients, densities and wave speeds for media 1 and 2

	λ (MPa)	μ (MPa)	ρ (kg m^{-3})	c_S (m s^{-1})	c_P (m s^{-1})
Medium 1	1126	562	1000	750	1500
Medium 2 (Soft Lung)	0.034	0.008	500	4	10
Medium 2 (Hard Lung 1)	0.200	0.050	500	10	24.5
Medium 2 (Hard Lung 2)	1	0.500	500	32	63
Medium 2 (Homogeneous)	1126	562	1000	750	1500

c_S and c_P are the pressure and shear waves speeds.

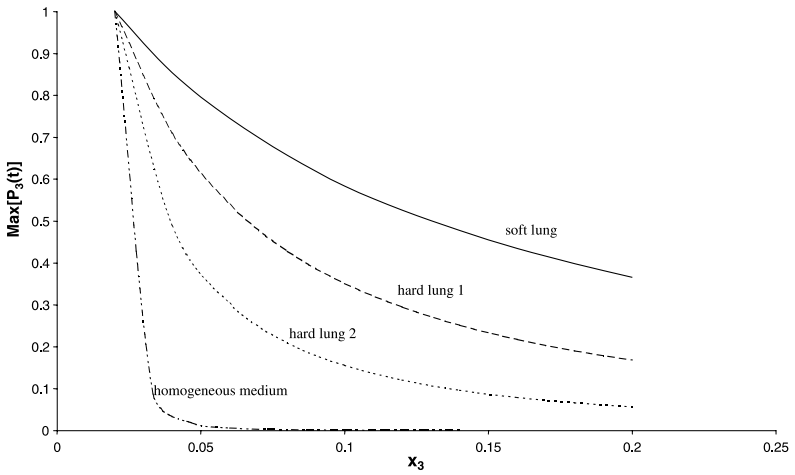

Fig. 3. Maximum of $P_3(t)$ at receivers on axis x_3 ($r = 0$), for different pairs of media, with respect to the distance from the interface. Data are normalized. The source is at $x_3 = 0$ and the interface at $x_3 = 0.02$.

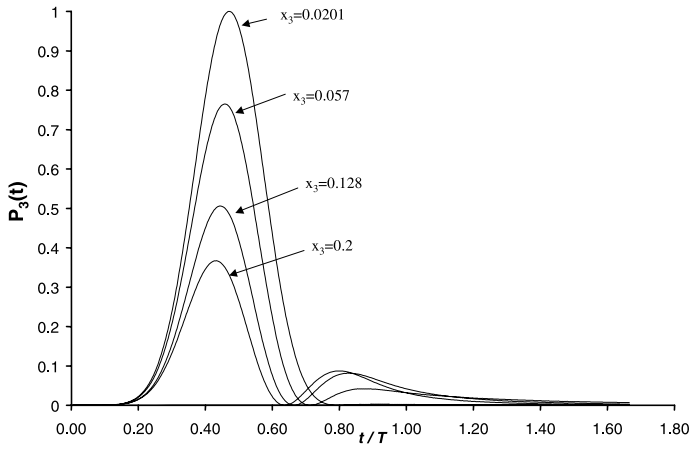

Fig. 4. Transient solutions $P_3(t)$ at receivers on axis x_3 ($r = 0$). Data are normalized with respect to the largest maximum at $x_3 = 0.0201$. Time is normalized with respect to the duration of the pulse (T) and the plots have been translated to make the arrival times at the different receivers coincide.

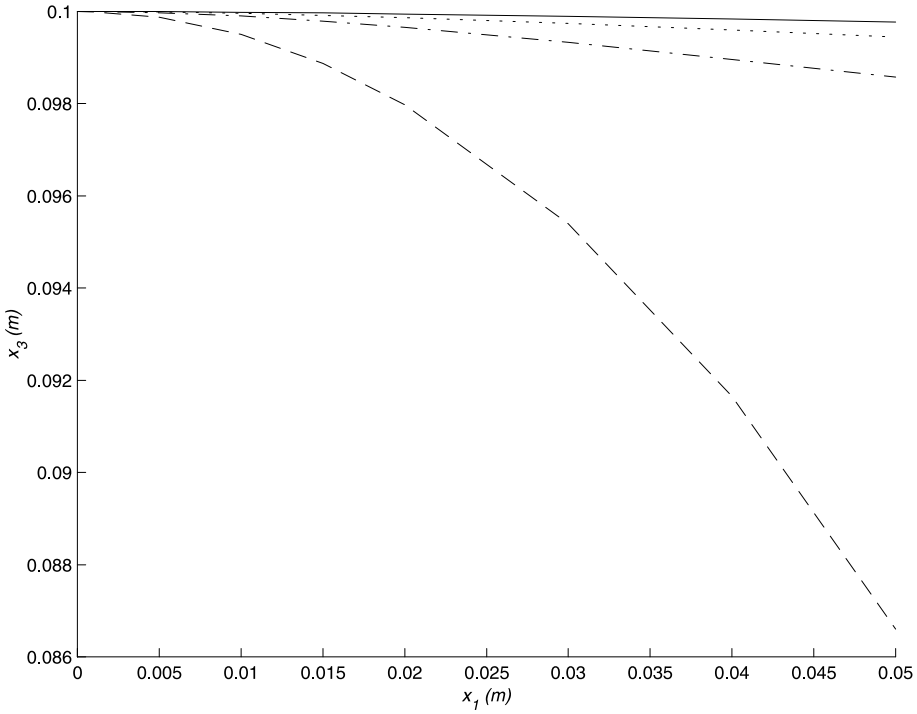

Fig. 5. P-waves fronts for four pairs of media (see Table 1): (——) "Homogeneous"; (—) "Soft lung"; (. . .) "Hard Lung 1"; (— - —) "Hard Lung 2".

are only small differences between their curvatures. It appears from Figs. 3 and 5 that the softer the lung, the weaker the front's curvature, and the decrease of the maximum of $P_3(t)$ is slower. Regarding the biomechanical problem, this result indicates that the weak acoustic coupling between the thoracic wall and

Table 2
Maximum of strain energy transmitted in medium 2 for different lung models (receiver at 1 mm above the interface)

Lung model	Maximum of $P_3(t)$
Soft Lung	0.20
Hard Lung 1	0.44
Hard Lung 2	1
Homogeneous	40.7

Data are normalized with repect to 'Hard Lung 2'.

the lung induces a relatively homogeneous solicitation of the lung along x_3. If the wave speeds in the lung and the thoracic wall were the same (see the "Homogeneous" case), the amplitude would decrease dramatically during the propagation inside the thorax. However, the discussion of the results concerning normalized amplitudes hides the differences between real amplitudes; indeed, the harder the second media, the better the coupling, and the more energy is carried in. For the four different pairs of media, Table 2 shows the maximum amplitudes of $P_3(t)$ transmitted in medium 2 at receivers located at 1 mm above the interface (values are scaled with respect to "Hard Lung 2").

It is to note that our lung model does not take into account the attenuation of the waves amplitudes due to the dissipation of energy in biological tissues. The influence of energy dissipation must be taken into account when dealing with high frequencies (dissipation is usually included in ultrasound waves propagation models) but lung models for the study of impact waves—associated with frequencies orders of magnitude lower than ultrasound waves—reported in the literature (Jahed et al., 1989; Stuhmiller et al., 1996; Bush and Challener, 1988) have not included dissipation effects. However, in the discussion of the results obtained with this model, we may include that: (i) shear waves are known to be more attenuated than longitudinal waves; (ii) the attenuation is proportional to the distance traveled by the wave; (iii) attenuation increases with frequency.

5.2. Repartition of energy in a model of the lung

In this subsection, we present results for the "Soft Lung" model (see Table 1).

Fig. 4 shows $P_3(t)$ for receivers on the $\mathbf{x}_3$-axis for the explosion source; plots have been translated so that, for each receiver on the $\mathbf{x}_3$-axis, the time origin corresponds to the arrival time of the wave; the normalized time $t/T = 1$ corresponds to the duration of the pulse. We note both the decrease in amplitude—which correlates with the results shown in Fig. 3—and the evolution of the shape of the transmitted pulse (for large values of x_3, the transient strain energy has two maxima of equal values), for most of the receivers, the response of the medium lasts longer than the pulse. The analytical solution for the strain energy in a homogeneous media shows a dependence in $\int \phi(t)\,\mathrm{d}t$, $\phi(t)$ and $\partial_t\phi(t)$ (where $\phi(t)$ is the pulse shape), the relative importance of each term evolves with the distance from the source. Such a dependence explains the change in the shape: a combination of far-field and near-field terms drives the pulse shape. From a physical point of view, the second lobe of the curves of Fig. 4—which increases with the distance from the source—may be thought of as an elastic return to the static stress value. Near the source, all the energy delivered by the source is used to put the media under static stress while far from the source, the static stress is negligible and the medium mainly undergoes a transient solicitation.

In Fig. 6, we show characteristic responses at a receiver in medium B for the explosion (Fig. 6a) and force sources (Fig. 6b) (sources of unit amplitude). We note that the energy arrives in two distinct bundles; the first is associated with P-waves and the second with S-waves. For the length and time scales of this study, the two bundles are well separated in time for receivers at a distance of the interface of more than a few

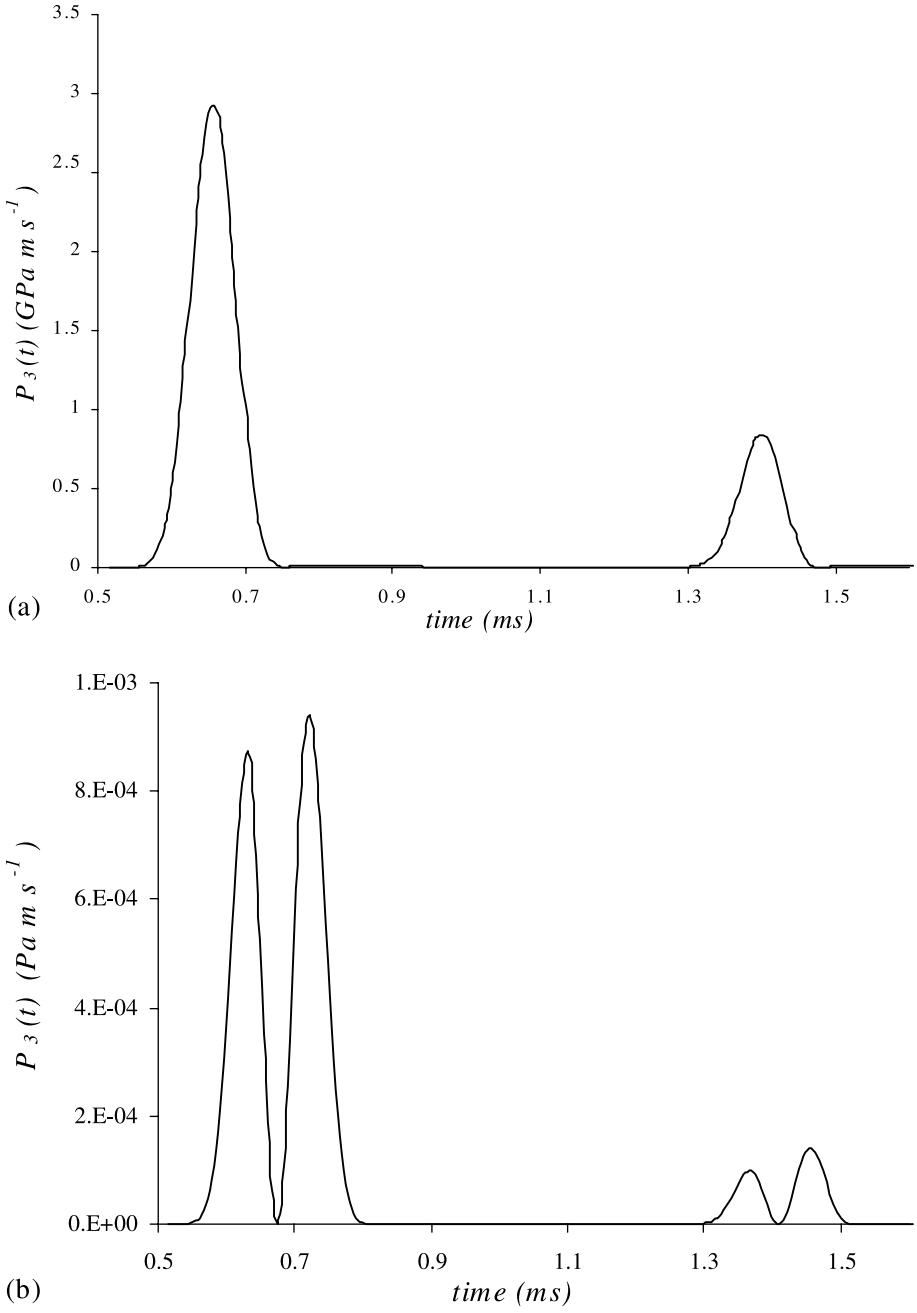

Fig. 6. Typical plots of $P_3(t)$ for a receiver located at $r = 0.01$ m and $x_3 = 0.025$ m for the explosion source (a) and the point force (b).

millimeters, thus we could always distinguish two maxima of energy flux (one for each bundle). The differences in the shape of $P_3(t)$ between the explosion and force sources are due to the different mechanical excitation at the source: for the explosion source, the medium expands at the source (just as if matter were

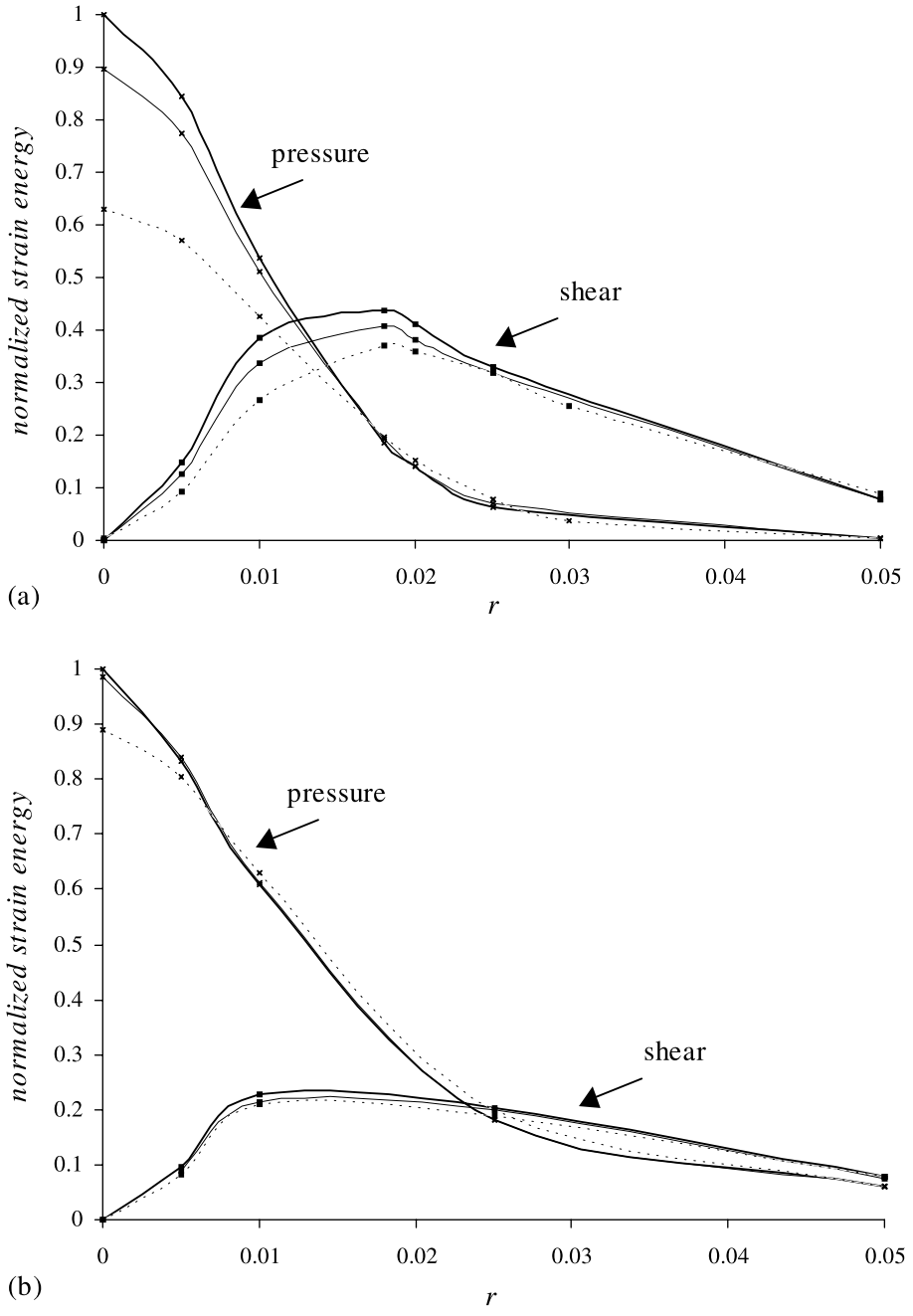

Fig. 7. Maximum of strain energies, associated with pressure and shear waves in medium 2 ("Soft Lung"), versus r $\left(r=\sqrt{x_1^2+x_2^2}\right)$ for some values of x_3: bold line $x_3 = 0.025$; thin continuous line $x_3 = 0.04$; dotted line $x_3 = 0.1$. (a) Explosion source; (b) point force. Data are normalized with respect to the largest maximum value. The source is at $x_3 = 0$ and the interface at $x_3 = 0.02$.

added at this point) at a rate given by the Blackman pulse, after the passage of the wave, the medium is under static stress; in contrast, in Case II, after the passage of the pulse, the medium returns at rest, this

explains why each bundle of energy of Fig. 6b shows two maxima. The relative amplitudes for the two models of sources have no physical signification.

According to the relation between the modulus of the Poynting vector and the density of strain energy underlined in Section 2 (see Eq. (44)), an approximation of the strain energy at receivers in medium 2 can be calculated for $P_3(t)$; the approximation is valid if the Poynting vectors (normal to the wave front) are parallel to the $\mathbf{x}_3$-axis, if the wave front has a weak curvature and if the amplitude of the wave varies slowly along the wave front. Fortunately, as shown in Figs. 3 and 5, the approximation is valid for the study of the "soft lung" model.

We distinguished in medium 2 the strain energy carried by P or S-waves; for the explosion source, only ray PS contributes to the S-strain energy, while for the force source, both rays PS and SS contribute to the S-strain energy, every other ray contribute to P-strain energy.

Fig. 7 shows the maximum of the strain energies, associated with P-waves and S-waves in medium 2—representing the lung—for Case I (Fig. 7a) and Case II (Fig. 7b) at receivers of coordinates (r, x_3). Each curve is the mapping of energy in planes (x_1, x_2) (since the wave fronts (see Fig. 5) are almost horizontal planes, each curve of Fig. 7 may be viewed as a mapping of energy along a wave front). The sources are placed at 2 cm below the interface. The strain energies are calculated for each point with the formula: $E_d^{\mathrm{P,S}} = \mathrm{Max}[P_3^{\mathrm{P,S}}(t)]/2c_{\mathrm{P,S}}$, where $\mathrm{Max}[P_3^{\mathrm{P,S}}(t)]$ is the maximum of one of the two parts (P or S-wave part) in plots like those shown in Fig. 6. Data were normalized with respect to the largest value. We note that the shear and pressure strain energies are of the same order of magnitude, the relative amplitude $E_d^{\mathrm{P}}/E_d^{\mathrm{S}}$ depends on r and is maximum at $r = 0$—indicating minimum conversion of energy at the vertical of the source (in the direction of x_3); for larger values of r, shear energy is larger than pressure energy. Energies were computed for points up to 8 cm above the interface, in this range, the energy maximum—located on the $\mathbf{x}_3$-axis—decreases slowly (37% and 11% in Cases I and II, respectively). In both cases, most of the energy is concentrated close to the $\mathbf{x}_3$-axis and 90% of the total energy (pressure and shear) is concentrated in a 8 cm-diameter tube of axis $\mathbf{x}_3$.

6. Conclusions

The three-dimensional transient wave propagation in a bimaterial has been investigated with an analytical method: the GR/CdH method. The formalism (adapted from Van Der Hijden, 1987) has been exposed in order to set all the elements needed to derive original solutions; readily implementable formulas, useful to calculate—without approximations—velocities and stresses (σ_{13}, σ_{23} and σ_{33}), for a given point source (explosion of force) of arbitrary time dependence, are given. The main original contributions—concerned with the method—of the current study are: (i) we present a closed form solution in a bimaterial, for receiver on the axis perpendicular to the interfaces and passing through the source (as far as the authors know, no equivalent solutions have been presented previously); this solution is useful to study transient phenomena in bimaterials and to test numerical methods of solution. (ii) we present the numerical schemes used for the numerical implementation of the exact three-dimensional GR/CdH method. (iii) we underline that the formalism commonly used to compute the mechanical response in stratified media—such as propagator matrix methods—readily yields an approximation to the strain energy, which is a quantity of a great interest for many engineering applications.

Numerical results are concerned with a biomechanical problem: the propagation of an impact wave inside the thorax modeled as a bimaterial representing the thoracic wall (medium 1) and the lung (medium 2). The model is suited to investigate the transmission of energy carried by waves, from the thoracic wall to the lung. The bimaterial under consideration is said to be weakly coupled in the sense that the mechanical

properties—and hence the wave speeds—of the two media are very different. This implies some specific properties: the wave fronts in medium 2 are almost plane (Fig. 5); and little energy is transmitted in medium 2, that is, much of the energy is reflected (Table 2). Furthermore, due to the characteristic lengths and time scales of the study and of the low waves speeds in medium 2, the P-waves and S-waves contributions are well separated in time (Fig. 6). We have not been concerned with the impact itself but with the propagation of the wave generated by the impact; we have investigated two models of sources to generate the wave motion in the thorax model: a buried point source of strain rate (explosion) and a point force at the free surface of the thorax model. The sources differ in their directivity: in a homogeneous medium, the energy radiated by the explosion source only depends on the distance to the source while for a point force, the energy radiated depends on the observer's orientation as well as on distance; in addition, the point force generates both P-waves and S-waves. Thus the distribution of shear and pressure strain energies associated with the explosion source (Fig. 7a) and with the force source (Fig. 7b) are different; both the directivity of the sources and types of waves emitted, together with the transmission coefficients at the interface, are responsible for the shapes of the curves.

We can summarize the results concerned with the biomechanical problem in the following three points. (a) The energy carried by the wave in the medium representing the lung decreases slowly as the wave penetrates inside the thorax, away from the thoracic wall. (b) The energy is concentrated around an axis passing through the impact point, as if it were propagating in a tube (ray trajectories and the variation with incidence of transmission coefficients, computed in the plane wave theory, qualitatively indicate the same tendency). When media 1 and 2 have closer properties than in the "Soft Lung" case (results not presented), energy is spread out in a wider part of medium 2 (not only close to axis $\mathbf{x}_3$), and the part of converted energy diminishes. (c) The use of the GR theory allowed us to discuss the relative contributions to strain energy of the pressure and shear waves: depending on the model of source, the amount of shear and pressure energies is different. It is interesting to note that more shear energy is present in medium 2 for the explosion source despite the fact that no shear wave is generated by the source in medium 1.

If the attenuation due to dissipation in soft tissues were taken into account, the concentration of energy around the $\mathbf{x}_3$-axis would probably be more important and the contribution of shear waves would probably be less; furthermore, the shape of the pulse would change in a different manner due to dispersion. However, no experimental data on the dissipation of waves in the lung are available for the frequencies of interest in this study.

Although the model of the thorax presented in this paper is very simple, the results yield a lot of valuable informations on the transmission of impact waves through the thoracic wall and the lung; however, the results are preliminary in the sense that the model needs to be fully validated by new experiments before it can be trusted. Working towards a more realistic model of the thorax, one should consider the following points: (i) the thorax is made of many tissues (ribs, fat...) which may be included with different material laws—but few experimental data on the response of tissues to impact waves are available—; (ii) the thoracic wall-lung interface is not plane; (iii) the condition of welded contact between the thoracic wall and the lung may not be appropriate because of the pleura. Using the same method of solution, we have been able to investigate the two last points; the results will be presented in another paper.

Acknowledgements

The authors would like to thank the 'Délégation Générale pour l'Armement' of the Minister of Defense of France for supporting this work.

Appendix A

Matrix appearing in the system giving by Eq. (4) of transform-domain equations

$$A = \begin{pmatrix} 0 & 0 & -ik_1 & 1/\mu & 0 & 0 \\ 0 & 0 & -ik_2 & 0 & 1/\mu & 0 \\ \dfrac{-i\lambda k_1}{\lambda+2\mu} & \dfrac{-i\lambda k_2}{\lambda+2\mu} & 0 & 0 & 0 & \dfrac{1}{\lambda+2\mu} \\ \rho + \dfrac{\mu(3\lambda+2\mu)}{\lambda+2\mu}k_1k_2 + \mu k^2 & \dfrac{\mu(3\lambda+2\mu)}{\lambda+2\mu}k_1k_2 & 0 & 0 & 0 & \dfrac{-i\lambda k_1}{\lambda+2\mu} \\ \dfrac{\mu(3\lambda+2\mu)}{\lambda+2\mu}k_1k_2 & \rho + \dfrac{\mu(3\lambda+2\mu)}{\lambda+2\mu}k_1k_2 + \mu k^2 & 0 & 0 & 0 & \dfrac{-i\lambda k_2}{\lambda+2\mu} \\ 0 & 0 & \rho & -ik_1 & -ik_2 & 0 \end{pmatrix}. \tag{A.1}$$

Matrix of eigenvectors of A and its inverse

$$D = \begin{pmatrix} c_P ik_1 & c_S s_3^S k_1 k^{-1} & -k_2 k^{-1} & c_P ik_1 & -c_S s_3^S k_1 k^{-1} & -k_2 k^{-1} \\ c_P ik_2 & c_S s_3^S k_2 k^{-1} & k_1 k^{-1} & c_P ik_2 & -c_S s_3^S k_2 k^{-1} & k_1 k^{-1} \\ -c_P s_3^P & ic_S k & 0 & c_P s_3^P & ic_S k & 0 \\ -2\mu c_P s_3^P ik_1 & -2\mu c_S \chi k_1 k^{-1} & \mu s_3^S k_2 k^{-1} & 2\mu c_P s_3^P ik_1 & -2\mu c_S \chi k_1 k^{-1} & -\mu s_3^S k_2 k^{-1} \\ -2\mu c_P s_3^P ik_2 & -2\mu c_S \chi k_2 k^{-1} & -\mu s_3^S k_1 k^{-1} & 2\mu c_P s_3^P ik_2 & -2\mu c_S \chi k_2 k^{-1} & \mu s_3^S k_1 k^{-1} \\ 2\mu c_P \chi & -2i\mu k c_S s_3^S & 0 & 2\mu c_P \chi & 2i\mu k c_S s_3^S & 0 \end{pmatrix}, \tag{A.2}$$

$$D^{-1} = \begin{pmatrix} -2\mu c_P s_3^P ik_1\epsilon_1 & -2\mu c_P s_3^P ik_2\epsilon_1 & 2\mu c_P \chi\epsilon_1 & c_P ik_1\epsilon_1 & c_P ik_2\epsilon_1 & -c_P s_3^P\epsilon_1 \\ -2\mu c_S \chi k_1 k^{-1}\epsilon_2 & -2\mu c_S \chi k_2 k^{-1}\epsilon_2 & -2i\mu k c_S s_3^S\epsilon_2 & c_S s_3^S k_1 k^{-1}\epsilon_2 & c_S s_3^S k_2 k^{-1}\epsilon_2 & ic_S k\epsilon_2 \\ \mu s_3^S k_2 k^{-1}\epsilon_3 & -\mu s_3^S k_1 k^{-1}\epsilon_3 & 0 & -k_2 k^{-1}\epsilon_3 & k_1 k^{-1}\epsilon_3 & 0 \\ 2\mu c_P s_3^P ik_1\epsilon_4 & 2\mu c_P s_3^P ik_2\epsilon_4 & 2\mu c_P \chi\epsilon_4 & c_P ik_1\epsilon_4 & c_P ik_2\epsilon_4 & c_P s_3^P\epsilon_4 \\ -2\mu c_S \chi k_1 k^{-1}\epsilon_5 & -2\mu c_S \chi k_2 k^{-1}\epsilon_5 & 2i\mu k c_S s_3^S\epsilon_5 & -c_S s_3^S k_1 k^{-1}\epsilon_5 & -c_S s_3^S k_2 k^{-1}\epsilon_5 & ic_S k\epsilon_5 \\ -\mu s_3^S k_2 k^{-1}\epsilon_6 & \mu s_3^S k_1 k^{-1}\epsilon_6 & 0 & -k_2 k^{-1}\epsilon_6 & k_1 k^{-1}\epsilon_6 & 0 \end{pmatrix}, \tag{A.3}$$

$$\epsilon_1 = -(2(\lambda+2\mu)s_3^P)^{-1} = -\epsilon_4, \quad \epsilon_2 = \epsilon_3 = -(2\mu s_3^S)^{-1} = -\epsilon_5 = -\epsilon_6, \tag{A.4}$$

where k and χ are respectively defined through $k^2 = k_1^2 + k_2^2$ and $\chi = 0.5s_S^2 + k^2$.

References

Aki, K., Richard, P.G., 1980. Quantitative Seismology: Theory and Methods. Freeman, San Fransisco.

Bush, I., Challener, S.A., 1988. Finite element modelling of non-penetrating thoracic impact. In: Proceedings of the International Research Council Biokinetics Impacts (IRCOBI), Bergish-gladbach.

Cetinkaya, C., Vakaris, A.F., 1996. Transient axisymetric stress wave propagation in weakly coupled layered structures. Journal of sound and vibration 194 (3), 389–416.

Eringen, A.C., Suhubi, E.S., 1975. In: Elastodynamics, vol. II, Linear Theory. Academic Press, New York.

Fung, Y.C., 1990. Strength, trauma and tolerance. In: Biomechanics Motion, Flow, Stress, and Growth. Springer-Verlag, New York.

Fung, Y.C., Yen, R.T., Tao, Z.L., Liu, S.Q., 1988. A hypothesis on the mechanism of trauma of lung tissue subjected to impact load. Journal of Biomechanichal Engineering 110, 50–56.

Grimal, Q., Watzky, A., Naili, S., 2001. Nonpenetrating impact on the thorax: a study of the wave propagation. Comptes Rendus de l'Académie des Sciences, Paris, Série IIb 329, 655–662.

Herrmann, R.B., 2001. Full wavenumber integration, computer program in seismology. Available from <http://www/eas/slu.edu/People/RBHerrmann/CPS20.html>.

Issacson, E., Keller, H.B., 1966. Analysis of Numerical Methods. John Wiley and Sons, New York.

Jahed, M., Lai-fook, S.J., Bhagat, P.K., Kraman, S.S., 1989. Propagation of stress waves in inflated sheep lungs. Journal of Applied Physiology 66, 2675–2680.

Johnson, L.R., 1974. Green's function for Lamb's problem. Geophysical Journal of the Royal Astronomical Society 37, 99–131.

Kennett, B.L.N., 1983. Seismic Wave Propagation in Stratified Media. Cambridge University Press.

Love, A.E.H., 1927. A Treatise on the Mathematical Theory of Elasticity. Dover Publication, New York.

Ma, C.C., Huang, K.C., 1996. Exact transient solutions of buried dynamic point forces for elastic bimaterials. International Journal of Solid Structures 33 (30), 4511–4529.

Nayfeh, A.H., Payfeh, A.H., 1995. Wave Propagation in Layered Anisotropic Media with Application to Composites. North Holland Publishing.

Pao, Y., Gajewski, R., 1977. The generalised ray theory and transient response of layered elastic solids. In: Mason, W.P. (Ed.), Physical Acoustics, 13, pp. 184–265.

Spencer, T.W., 1960. The method of generalized reflection and transmission coefficients. Geophysics 25, 625–641.

Stuhmiller, J.H., Ho, K.H., Vander Vorst, M.J., Dodd, K.T., Fitzpatrick, T., Mayorga, M., 1996. A model of blast overpressure injury to the lung. Journal of Biomechanics 29 (2), 227–234.

Van Der Hijden, J.H.M.T., 1987. Propagation of Transient Elastic Waves in Stratified Anisotropic Media. North Holland Series in Applied Mathematics and Mechanics, vol. 32.

Yang, K.H., Wang, K.H., 1998. Finite element modeling of the human thorax. Available from <http://wwwils.nlm.nih.gov/research/visible/vhpconf98/AUTHORS/YANG/YANG.HTM>.

Yen, R.T., Fung, Y.C., Liu, S.Q., 1988. Trauma of the lung due to impact load. Journal of Biomechanics 21, 745–753.